Investigating the effects of random data errors on the waveform-based moment tensor inversion

Geophysical Journal International

Geophys. J. Int. (2022) **229,** 97–109
Advance Access publication 2021 November 12
GJI Seismology

https://doi.org/10.1093/gji/ggab445

Investigating the effects of random data errors on the waveform-based moment tensor inversion

K. Moghtased-Azar [1], H. Zeynal-Kheiri [2] and M. Hallo [3]

[1] *Department of Geomatics Engineering, Faculty of Civil Engineering, University of Tabriz, Tabriz* 5166616471, *Iran. E-mail: moghtased@tabrizu.ac.ir*
[2] *School of Surveying and Geospatial Engineering, College of Engineering, University of Tehran, Tehran* 1439957131, *Iran*
[3] *Swiss Seismological Service (SED), ETH Zürich, Zürich* 8092, *Switzerland*

Accepted 2021 October 26. Received 2021 October 16; in original form 2021 August 7

SUMMARY

The linear Gauss–Markov model for waveform-based moment tensor inversion often relies on the overdetermined least-squares method. It needs a proper stochastic model of the observables for accurate and precise estimates of the unknown parameters. Furthermore, estimating the level and distribution of random errors in the observed waveforms is challenging due to assessing the minimum-variance unbiased estimator (MVUE). Hence, according to the considerable effects of random data errors in assessing the uncertainty of the moment tensor components, this paper aims to describe an MVUE of the data covariance matrix and its application on uncertainty quantification of the moment tensor. The used mathematical prescription allows us to use the covariance matrix for the three-component noise records at every station and all possible cross-correlations among the recorded noise wavefield. To illustrate the proposed method's performance, we conducted tests with synthetic data using configuration of the 2018 M_w 6.8 Zakynthos (Ionian Sea, Greece) earthquake. Both uncorrelated and correlated random noise traces were added to the synthetic waveform data in amounts between 5 and 20 per cent of the maximum amplitude. In order to test the efficiency of the method, we considered three different structures of covariance matrix: (i) diagonal matrix (contains a variance of individual measurements at seismic stations), (ii) block-diagonal matrix (considering cross-covariance among three components at each station), and (iii) full covariance matrix. Test results are presented by comparison of the moment tensor inversion outcomes with known noise levels of generated synthetic data and with synthetic focal mechanisms, the ability of the estimated full covariance matrix in illustrating the minimum variance of parameters (namely, minimum posterior uncertainties), unbiased of the parameters, and values of the cross-correlations between the components of each station and also among stations. Finally, we applied the method to the real waveforms of the Zakynthos earthquake having inferred focal mechanism of strike/dip/rake angles 13/40/171 (deg) with 33 per cent double couple (DC) and −61 per cent compensated linear vector dipole component (CLVD). The focal mechanism solution has strike/dip/rake angles 19/34/177 (deg) with 69 per cent DC and −23 per cent CLVD when using our estimated full covariance matrix.

Key words: Statistical methods; Time-series analysis; Waveform inversion; Statistical seismology.

1 INTRODUCTION

A seismic source model can be formulated in the point-source approximation, where it is kinematically described by the seismic moment tensor ($\boldsymbol{M}$) (Aki & Richard 2002). In terms of force couples, $\boldsymbol{M}$ represents any source of deformation in an elastic media. The tensor $\boldsymbol{M}$ of pure shear earthquakes corresponds to a simple double couple (DC) of forces. The $\boldsymbol{M}$ contains information about the released seismic moment of the earthquake and simplified fault geometry (strike, dip and rake angles of nodal planes). Moreover, $\boldsymbol{M} \in \mathbb{R}^{3\times3}$ as a second-order symmetric tensor is an essential tool for statistical inferences about fault orientation and the principal components of the local stress tensor if many focal mechanisms are available.

According to the representation theorem, the observed ground motions are linearly related to the moment tensor components

through the Green's functions, which could be fully described based on crustal structure, locations of point source, station, and frequency range (e.g. Kikuchi & Kanamori 1986). However, any systematic error (e.g. clock drift, sizeable azimuthal gap, wrong source location, inaccurate crustal models) or random error (e.g. instrumental noise, sensor misalignment) may lead to misleading inference of source parameters. The tensor $\boldsymbol{M}$ determinations need to be improved, particularly concerning the assessment of the reliability of the solution and associated uncertainties (e.g. Tarantola & Valette 1982; Valentine & Trampert 2012). Typically, when dealing with large seismic events, the modelling error (error of Green's functions) is of the primary importance (e.g. Hallo *et al.* 2017). The random data error has importance for mid-size or small-size earthquakes (Vackář *et al.* 2017).

On the one hand, since the wavefield still consists of propagating seismic waves, one cannot neglect the correlation between recorded ground-motion components at a single station. On the other hand, we can assume zero correlations between the noise recordings at different stations. It is a valid assumption for stations that are far away from each other and for high-frequency seismic noise so that various noise sources dominate the recording at different stations. For stations close to each other, seismic arrays, collocated sensors and low-frequency noise, it might be useful to consider cross-covariance between stations, each of them with three components (Vackář *et al.* 2017).

In this paper, we focus on estimating random data errors (non-systematics effects) and their effect on uncertainty of $\boldsymbol{M}$ and, consequently, errors of the strike, dip and rake. Over the past two decades, considerable efforts have been dedicated to estimating data error. For instance, Vasco (1990) proposed that the data error value is the maximum between the background noise level (σ) and the misfit between pairs of observed (d) and synthetic waveforms (s), namely $\sigma_e = \max(\sigma, |d - s|)$. The term $|d - s|$ includes both data error and modelling error. Šílený *et al.* (1992) developed a method to retrieve source parameters from weak, local and noisy waveforms.

Wéber (2006) developed a probabilistic method to determine the simultaneously earthquake-source mechanism, hypocentral location and source time function (STF) from the inversion of short-period waveform data of weak local events. The procedure considers the effects of the random noise in the seismograms, the uncertainty of the hypocentre determined from arrival times and the inaccurate knowledge of the velocity structure while estimating the error affecting the derived focal parameters.

Monelli *et al.* (2009) also highlighted the difference between random error and systematic error, but given the impossibility to compute either, opted for an empirical approach where the error was obtained from the data-synthetics misfit. Yagi & Fukahata (2008, 2011) proposed incorporating a full data covariance matrix during inversion for earthquake slip distribution. They computed the covariance matrix from the misfit between observed and synthetic waveforms and included it in the inverse problem to iteratively improve the estimate of the model parameters. Also, Monelli *et al.* (2009) have pointed that a feasible approach to derive a data covariance matrix would be to analyse the portion before the *P*-wave arrival of each trace and to assume this portion to be representative of the seismic noise.

Also, Zahradník & Custódio (2012) presented a method to assess the uncertainty of $\boldsymbol{M}$ based on the standard theory of linear inverse problems. They computed the uncertainty of the DC part of $\boldsymbol{M}$, then mapped it into uncertainties of the strike, dip and rake. The inputs were the source and station locations, the crustal model, the frequency band of interest and an estimate of data error. They reported that it was impossible to accurately and independently obtain random error (data error) and systematic error (e.g. modelling error). Namely, they used data error as a misfit between measured and synthetic waveforms (whether the data-synthetics inconsistencies resulted from the incorrect Green's function or seismograms). According to Zahradník & Custódio (2012), the noise term usually produces data error values in the order of 1–10 per cent of the data amplitude (noisier data are normally left out of the inversion).

As another kind of application of data error estimation in seismic source inversions, Duputel *et al.* (2012) used three different types of data covariance matrix in uncertainty estimation: (i) diagonal covariance, (ii) diagonal covariance matrix whose elements correspond to a measured noise level, (iii) including the non-diagonal terms in the covariance matrix due to the interdependence of observational errors. The non-diagonal terms, as the resulting covariances between neighbour data samples, were incorporated by considering an exponential decay defined by a correlation length chosen as the shortest period content after filtering.

Minson *et al.* (2013) used data covariance data in model prediction error of the Bayesian inversion for finite fault earthquake source models. Sokos & Zahradník (2013) estimated the data error as the posterior variance factor $\hat{\sigma}^2 = \sum(d - s)^2/\nu$, where ν are the degrees of freedom (or redundancy) and are equal to the number of independent data minus the number of the inverted parameters.

Mustać & Tkalčić (2016) developed a nonlinear moment tensor inversion method in a probabilistic Bayesian framework that also accounts for data covariance data. Vackář *et al.* (2017) used covariance matrix of the data for centroid moment tensor (CMT) inversion using the lagged covariance function. However, they have assumed no correlation between different stations. Duputel *et al.* (2014) used the data covariance matrix to incorporate the impact of uncertainties in fault slip inverse problems. Hallo *et al.* (2017) have presented the application of the innovative Bayesian full-waveform CMT inversion method, which considered the uncertainty of the velocity model. Their approach made reliably assess the uncertainty of the CMT parameters, including the centroid position. Spudich *et al.* (2019) verified variability in synthetic earthquake ground motions caused by source variability and errors in wave propagation models.

As seen, due to incomplete knowledge of data error and resolving it, numerous methods of estimations have been applied in many seismological applications. An adequate statistical model is thus needed to arrive at a proper description of the estimator's quality. Under the assumption of Gaussian data errors, realistic covariance matrix allows one, first, to obtain the best (minimum variance or namely minimum uncertainties) linear unbiased estimator of the source model parameters; second, to determine their realistic uncertainties; and, third, along with the distribution of the data, to correctly perform hypothesis testing and assess quality control measures such as reliability.

Hence, considering the effects of random data errors in assessing the uncertainty of the $\boldsymbol{M}$ components, the goal of this paper is to introduce a minimum-variance unbiased estimator of the covariance matrix of the data and its application on uncertainty quantification of the moment tensor. This assumption allows us to estimate the covariance matrix of the data for the three-component noise records at every station and all possible cross-correlations among the recorded noise wavefield. Then we include the matrix in the $\boldsymbol{M}$ calculation, obtain the covariance matrix of model parameters and estimate their posterior probability density function. It is validated

in synthetic tests and applied on observed waveform data from the 2018 M_w 6.8 Zakynthos earthquake (Greece).

The paper is structured as follows. First, we describe the formulation of the moment tensor inversion. Second, we construct a maximum likelihood (ML) method for estimating the covariance matrix. Third, numerical examples are presented to evaluate the (co)variance estimation method on synthetic and real data sets. The last section draws several conclusions.

2 FORMULATION OF THE MOMENT TENSOR INVERSION

We start from the particular consistent linear Gauss–Markov model: let us assume a point seismic source model for a fixed earthquake origin time and location (embedded in a given 1-D velocity model), which generates ground motion in terms of (Zahradník & Custódio 2012)

$$d_i(t) = \sum_{j=1}^{\mathcal{X}} G_{ij}(t) m_j + e_i(t), \tag{1}$$

where $\mathbf{d}(t) \in \mathbb{R}^{N\times 1}$ is the vector of displacement waveforms, $\mathbf{G}(t) \in \mathbb{R}^{N\times\mathcal{X}}$ is the matrix of Green's functions (based on crustal structure, source location and station location, which is called design matrix of rank$(\mathbf{G}) = \mathcal{X}$, where $\mathcal{X}$ is the number of independent components of tensor $\boldsymbol{M}$ (depending on whether using full moment tensor $\mathcal{X} = 6$ or using its deviatoric part $\mathcal{X} = 5$), and $\mathbf{m} \in \mathbb{R}^{\mathcal{X}\times 1}$ is the vector of unknown parameters that fully determine $\boldsymbol{M}$. Further, $\mathbf{e}(t) \in \mathbb{R}^{N\times 1}$ is the vector of measurement errors which is generally assumed to be random with zero mean $\mathrm{E}\{\mathbf{e}\} = 0$, where $\mathrm{E}\{.\}$ denotes expectation operator, and $\mathrm{cov}\{\mathbf{d}\} = \mathrm{cov}\{\mathbf{e}\}$ is the symmetric positive-definite covariance matrix, where $\mathrm{cov}\{.\}$ denotes dispersion matrix or covariance matrix. Furthermore, we have assumed that the source–time function of the $\boldsymbol{M}$ is known. In terms of a special Gauss–Markov model, for a given observed values ($\mathbf{d}$), a linear estimator $\hat{\theta}$ has minimum-variance unbiased estimator (MVUE) properties if it has a lower variance than any other unbiased estimator for all possible values of the parameter (Grafarend & Awange 2012):

(i) *Unbiasedness*. The estimator $\hat{\theta}$ is said to be an unbiased estimator of θ if and only if the expectation of the estimation error is zero, $\mathrm{E}\{\hat{\theta}\} = \theta$. An estimator which is not unbiased is said to be biased, and the difference $\mathrm{E}\{\hat{\epsilon}\} = \mathrm{E}\{\hat{\theta}\} - \theta$ is called the bias of the estimator. Therefore, the bias size is a measure of closeness of $\hat{\theta}$ to θ. The mean error $\mathrm{E}\{\hat{\epsilon}\}$ is a measure of closeness that makes use of the first moment of the distribution of $\hat{\theta}$.

(ii) *Minimum variance (best)*. A second measure of closeness of the estimator to θ is the mean squared error (MSE), $\mathrm{MSE} = \mathrm{E}\{(\hat{\theta} - \theta)^{\mathrm{T}}(\hat{\theta} - \theta)\}$, which is defined as $\arg\min_{\theta}(\mathrm{MSE})$. If we compare different estimators by looking at their respective MSEs, we would prefer one with a small or the smallest MSE. It is a measure of closeness that also makes use of the second moment of the distribution of $\hat{\theta}$, namely $\mathrm{cov}\{\hat{\theta}\}$. The best estimator, in the absence of biases, therefore is of minimum variance.

(iii) *Maximum likelihood*. The goal of ML estimation is to find the values of the model parameters $\mathbf{m}$ that maximize the likelihood function over the parameter space, that is $\hat{\theta} = \arg\max_{\theta} \mathcal{L}_{\boldsymbol{M}}(\theta, \mathbf{d})$, where $\mathcal{L}_{\boldsymbol{M}}$ is called the likelihood function. If we were to compare different estimators by looking at their respective values for the above probability, we would prefer one with a large or the most considerable probability.

3 MAXIMUM LIKELIHOOD METHOD FOR ESTIMATING THE COVARIANCE MATRIX

The symmetric positive-definite matrix $\mathrm{cov}\{\mathbf{d}\}$ is assumed to consist of p' *estimable variance* components (associated with positive values) and $p - p'$ *estimable covariance* components (associated with positive or negative values) as follows:

$$\mathrm{cov}\{\mathbf{d}\} = \sum_{i=1}^{p'} \sigma_i^2 \mathbf{T}_i + \sum_{i=p'+1}^{p} \sigma_i \mathbf{T}_i, \tag{2}$$

where $\mathbf{T}_i$ is the given cofactor matrices as *positive (semi-)definite* matrices for $\{\sigma_i |\ i \in \{1, \ldots, p'\}\}$ and given *symmetrical* matrices for $\{\sigma_i |\ i \in \{p' + 1, \ldots, p\}\}$. The matrices $\{\mathbf{T_i} |\ i \in \{1, \ldots, p\}\}$ should be linearly independent and symmetric. For instance, if σ_i^2 corresponds to the variances of ith station, then $\mathbf{T}_i$ is the zero matrix, except for the ith block-diagonal elements being equals to unities:

$$\mathbf{T}_i = \begin{bmatrix} \mathbf{0} & \cdots & \mathbf{0} & \cdots & \mathbf{0} \\ \vdots & \ddots & \vdots & & \vdots \\ \mathbf{0} & \cdots & \mathbf{I} & \cdots & \mathbf{0} \\ \vdots & & \vdots & \ddots & \vdots \\ \mathbf{0} & \cdots & \mathbf{0} & \cdots & \mathbf{0} \end{bmatrix}. \tag{3}$$

In the same manner, if σ_k corresponds to the covariances between ith station and jth station, then $\mathbf{T}_k$ would be

$$\mathbf{T}_k = \begin{bmatrix} \mathbf{0} & \cdots & \mathbf{0} & \cdots & \mathbf{0} & \cdots & \mathbf{0} \\ \vdots & \ddots & \vdots & & \vdots & & \vdots \\ \mathbf{0} & \cdots & \mathbf{0} & \cdots & \mathbf{I} & \cdots & \mathbf{0} \\ \vdots & & \vdots & \ddots & \vdots & & \vdots \\ \mathbf{0} & \cdots & \mathbf{I} & \cdots & \mathbf{0} & \cdots & \mathbf{0} \\ \vdots & & \vdots & & \vdots & \ddots & \vdots \\ \mathbf{0} & \cdots & \mathbf{0} & \cdots & \mathbf{0} & \cdots & \mathbf{0} \end{bmatrix}. \tag{4}$$

The above listed cofactor matrices are linearly independent and therefore the variance components $\{\sigma_i |\ i \in \{1, \ldots, p'\}\}$ and covariance components $\{\sigma_k |\ k \in \{p' + 1, \ldots, p\}\}$ are simultaneously estimable.

Furthermore, the vector of variance and covariance components $\boldsymbol{\sigma} \in \mathbb{R}^{p\times 1}$ can be described by

$$\boldsymbol{\sigma} := [\sigma_1^2, \sigma_2^2, \ldots, \sigma_{p'}^2, \sigma_{p'+1}, \sigma_{p'+2}, \ldots, \sigma_p]^{\mathrm{T}}. \tag{5}$$

Under the assumption of Gauss–Laplace normal distribution of the observation vector, namely $\mathbf{d} \sim \mathcal{N}(\mathbf{Gm}, \mathrm{cov}\{\mathbf{d}\})$, the probability density function of the observations $p(\mathbf{d}|\mathbf{m}, \mathbf{G})$ is given by the likelihood function:

$$\mathcal{L}_{\boldsymbol{M}}(\mathbf{m}, \boldsymbol{\sigma}|\mathbf{d}) := p(\mathbf{d}|\mathbf{m}, \boldsymbol{\sigma}) = (2\pi)^{-0.5N} |\mathrm{cov}\{\mathbf{d}\}|^{-0.5} \times \exp\left(-0.5(\mathbf{d} - \mathrm{E}\{\mathbf{d}\})^{\mathrm{T}} \mathrm{cov}\{\mathbf{d}\}^{-1} (\mathbf{d} - \mathrm{E}\{\mathbf{d}\})\right), \tag{6}$$

where determinant of a matrix is denoted by $|\ \ |$. Maximizing $\mathcal{L}_{\boldsymbol{M}}(\mathbf{m}, \boldsymbol{\sigma}|\mathbf{d})$ with respect to unknown parameters of $\mathbf{m}$ and $\boldsymbol{\sigma}$ yields to equations that have to be solved to yield ML estimators of $\mathbf{m}$ and of $\boldsymbol{\sigma}$.

One drawback with covariance component estimation via the usual ML approach is that it takes no account of the loss in degrees of freedom needed to estimate the unknown parameter $\mathbf{m}$, and is generally biased. To overcome this situation, the restricted

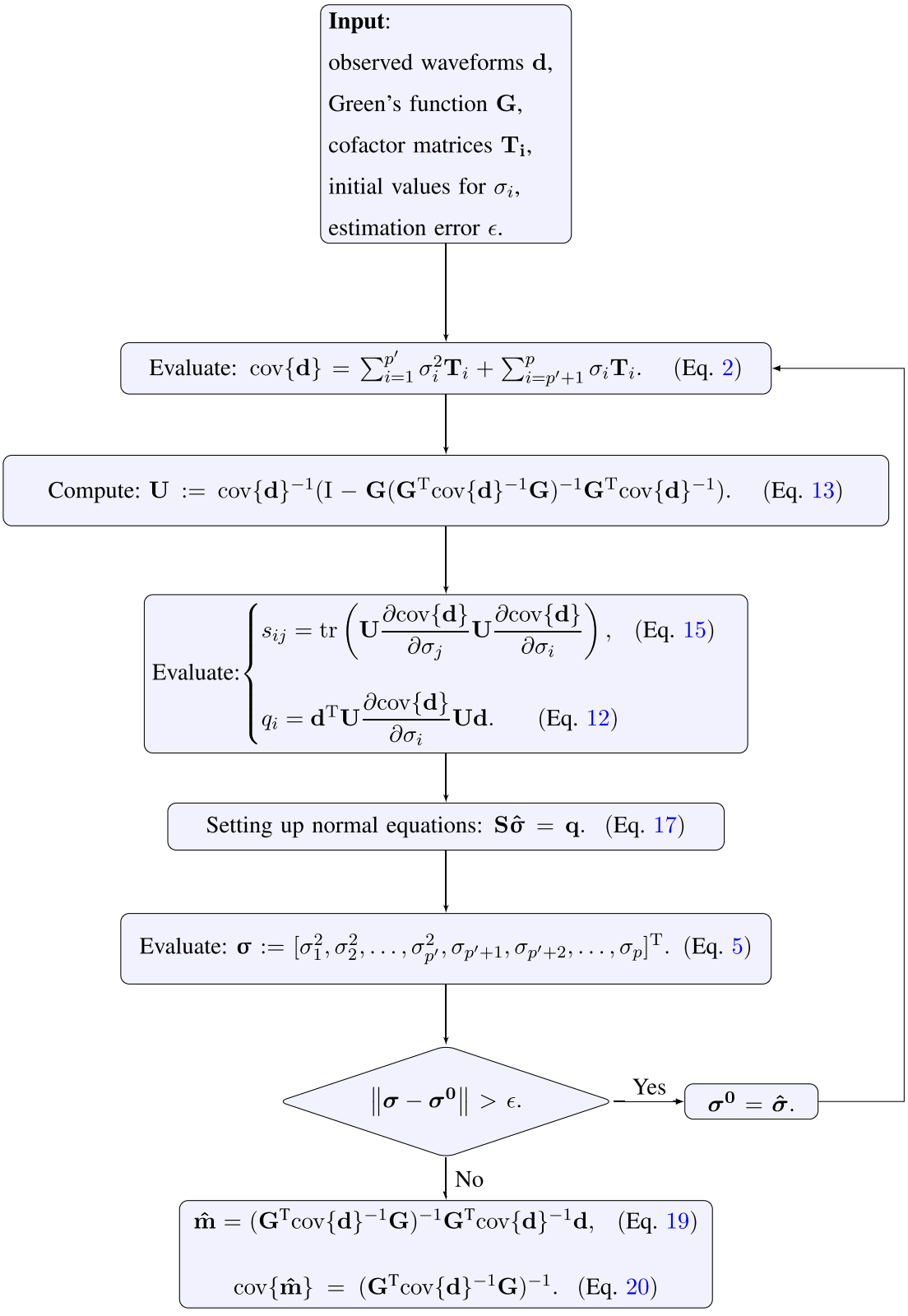

Figure 1. Flowchart showing the implementation of data covariance matrix estimation.

ML (REML) estimator has been suggested (Koch 1986, 1999). The REML method uses the linear transformation that maps the observable vector $\mathbf{d} \in \mathbb{R}^{N\times 1}$ to new observable vector $\tilde{\mathbf{d}} := \mathbf{P}\mathbf{d}$ in which $\tilde{\mathbf{d}} \in \mathbb{R}^{N\times 1}$ and $\mathbf{P} \in \mathbb{R}^{N\times N}$. The transformation matrix is given by $\mathbf{P} := [\mathbf{B}^{\mathrm{T}} \quad \mathrm{cov}\{\mathbf{d}\}^{-1}\mathbf{G}]^{\mathrm{T}}$ subject to $\mathbf{B}\,\mathbf{G} = \mathbf{0}$, where $\mathbf{B} \in \mathbb{R}^{(N-\mathcal{X})\times N}$ with $\mathrm{rank}(\mathbf{B}) = N - \mathcal{X}$. Consequently, REML considers the likelihood function of the distribution of $\tilde{\mathbf{d}}$ associated with

$$\begin{cases} \mathrm{E}\{\tilde{\mathbf{d}}\} := \mathbf{P}\mathrm{E}\{\mathbf{d}\} \\ \mathrm{cov}\{\tilde{\mathbf{d}}\} = \mathbf{P}\mathrm{cov}\{\mathbf{d}\}\mathbf{P}^{\mathrm{T}} \end{cases}. \tag{7}$$

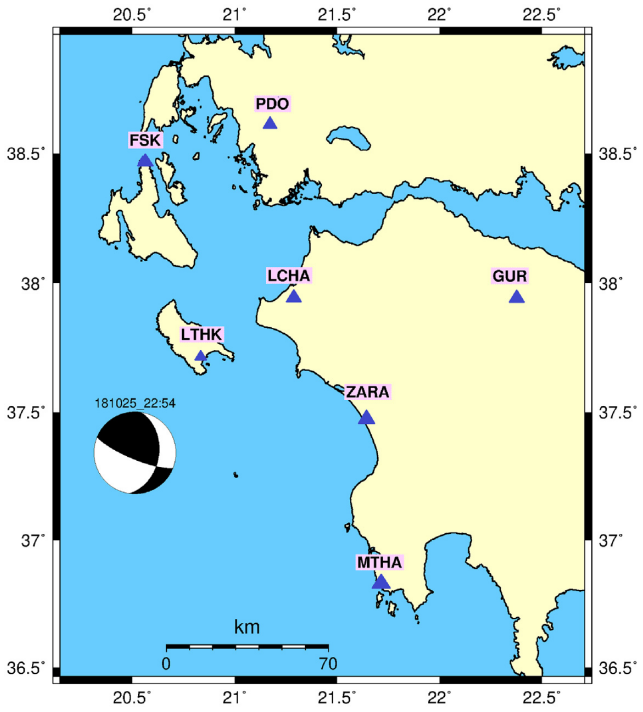

Figure 2. Location map of the 2018 Zakynthos earthquake and used strong-motion stations: LCHA, ZARA and MTHA belong to the National Observatory of Athens (NOA) strong-motion network, whereas LTHK, FSK, PDO and GUR are operated by the University of Patras and the Charles University which were already used by Sokos *et al.* (2020).

Accordingly, the likelihood function $\mathcal{L}_M(\mathbf{m}, \boldsymbol{\sigma}|\tilde{\mathbf{d}})$ can be described by

$$\mathcal{L}_M(\mathbf{m}, \boldsymbol{\sigma}|\tilde{\mathbf{d}}) := (2\pi)^{-0.5N}|\mathbf{P}\mathrm{cov}\{\mathbf{d}\}\mathbf{P}^{\mathrm{T}}|^{-0.5} \times \exp\left(-0.5(\tilde{\mathbf{d}} - \mathrm{E}\{\tilde{\mathbf{d}}\})^{\mathrm{T}}(\mathbf{P}\mathrm{cov}\{\mathbf{d}\}\mathbf{P}^{\mathrm{T}})^{-1}(\tilde{\mathbf{d}} - \mathrm{E}\{\tilde{\mathbf{d}}\})\right), \tag{8}$$

where $\mathbf{P}\mathrm{cov}\{\mathbf{d}\}\mathbf{P}^{\mathrm{T}}$ is the positive-definite matrix. By using eqs (7) and (8), the likelihood function $\mathcal{L}_M(\mathbf{m}, \boldsymbol{\sigma}|\tilde{\mathbf{d}})$ can be derived as the product of two likelihood functions of $\mathcal{L}_1(\boldsymbol{\sigma}|\mathbf{d})$ and $\mathcal{L}_2(\mathbf{m}, \boldsymbol{\sigma}|\mathbf{d})$ in which the former depends only on $\boldsymbol{\sigma}$, whereas the latter contains both $\boldsymbol{\sigma}$ and $\mathbf{m}$. Hence, this likelihood function will be used to estimate the unknown variance and covariance components $\boldsymbol{\sigma}$.

For a given $\mathrm{cov}\{\mathbf{d}\}$, $\hat{\mathbf{m}} := \arg\max_{\mathbf{m}} \mathcal{L}_2(\mathbf{m}, \boldsymbol{\sigma}|\mathbf{d})$ leads to estimate $\hat{\mathbf{m}}$ through solving the normal equations:

$$\mathbf{G}^{\mathrm{T}}\mathrm{cov}\{\mathbf{d}\}^{-1}\mathbf{G}\hat{\mathbf{m}} = \mathbf{G}^{\mathrm{T}}\mathrm{cov}\{\mathbf{d}\}^{-1}\mathbf{d}. \tag{9}$$

These are the well-known normal equations of the ML estimate (MLE). That means that in the case of normally distributed observations, the solution of the MLE is identical to the solution of the least-squares method, which is applied to the unknown parameters $\hat{\mathbf{m}}$ of the Gauss–Markov model. Furthermore, the maximization of the first likelihood function $\hat{\boldsymbol{\sigma}} := \arg\max_{\boldsymbol{\sigma}} \ln \mathcal{L}_1(\boldsymbol{\sigma}|\boldsymbol{d})$ is equivalent to maximization of

$$\ln \mathcal{L}_1(\boldsymbol{\sigma}|\mathbf{d}) := -0.5(N - \mathcal{X})\ln(2\pi) - 0.5\ln|\mathbf{B}\mathrm{cov}\{\mathbf{d}\}\mathbf{B}^{\mathrm{T}}| - 0.5(\mathbf{B}\mathbf{d})^{\mathrm{T}}(\mathbf{B}\mathrm{cov}\{\mathbf{d}\}\mathbf{B}^{\mathrm{T}})^{-1}(\mathbf{B}\mathbf{d}), \tag{10}$$

which yields nonlinear equation for the MLEs of the (co)variance components as

$$\boldsymbol{f}(\boldsymbol{\sigma}) := \mathbf{v} - \mathbf{q} = \mathbf{0}, \tag{11}$$

in which

$$\begin{cases} q_i := \mathbf{d}^{\mathrm{T}}\mathbf{U}\dfrac{\partial \mathrm{cov}\{\mathbf{d}\}}{\partial \sigma_i}\mathbf{U}\mathbf{d}, \\ v_i := \mathrm{tr}\left(\mathbf{U}\dfrac{\partial \mathrm{cov}\{\mathbf{d}\}}{\partial \sigma_i}\right), \end{cases} \tag{12}$$

where

$$\mathbf{U} := \mathbf{B}^{\mathrm{T}}(\mathbf{B}\mathrm{cov}\{\mathbf{d}\}\mathbf{B}^{\mathrm{T}})^{-1}\mathbf{B} = \mathrm{cov}\{\mathbf{d}\}^{-1}(\mathrm{I} - \mathbf{G}(\mathbf{G}^{\mathrm{T}}\mathrm{cov}\{\mathbf{d}\}^{-1}\mathbf{G})^{-1}\mathbf{G}^{\mathrm{T}}\mathrm{cov}\{\mathbf{d}\}^{-1}), \tag{13}$$

subject to $\mathbf{U}\mathbf{G} = \mathbf{0}$ and $\mathbf{U} \in \mathbb{R}^{N\times N}$. The Newton–Raphson method of solving a nonlinear equation of the type eq. (11) leads

$$\mathbf{S}(\boldsymbol{\sigma} - \boldsymbol{\sigma}_0) = \mathbf{q} - \mathbf{v}, \tag{14}$$

where

$$s_{ij} = \mathrm{tr}\left(\mathbf{U}\frac{\partial \mathrm{cov}\{\mathbf{d}\}}{\partial \sigma_j}\mathbf{U}\frac{\partial \mathrm{cov}\{\mathbf{d}\}}{\partial \sigma_i}\right). \tag{15}$$

However, matrix $\mathbf{S}$ and vectors $\mathbf{q}$ and $\mathbf{v}$ have to be evaluated at approximation values $\boldsymbol{\sigma}_0$. Furthermore, using the Taylor series and restricting it to the linear terms,

$$\mathrm{cov}\{\mathbf{d}\}_{\boldsymbol{\sigma}^0} = \mathrm{cov}\{\mathbf{d}\}_{\boldsymbol{\sigma}^e} + \sum_{i=1}^{p}\frac{\partial \mathrm{cov}\{\mathbf{d}\}_{\boldsymbol{\sigma}}}{\partial \sigma_i}\bigg|_{\boldsymbol{\sigma}=\boldsymbol{\sigma}^e}(\sigma_i^0 - \sigma_i^e), \tag{16}$$

around the point of expansion $\boldsymbol{\sigma} = \boldsymbol{\sigma}^e$, we get the system of equations for the estimates of (co)variance components:

$$\mathbf{S}\hat{\boldsymbol{\sigma}} = \mathbf{q}. \tag{17}$$

Such estimator is therefore unbiased, of minimum variance and restrictedly of ML (Koch 1986). Consequently, the associated (co)variance matrix of vector $\hat{\boldsymbol{\sigma}}$ would be

$$\mathrm{cov}\{\hat{\boldsymbol{\sigma}}\} = 2\mathbf{S}^{-1}. \tag{18}$$

Xu *et al.* (2007) discussed the estimability analysis of variance and covariance components and proved that they were not *estimable* for a fully unknown variance–covariance matrix. They have highlighted that only up to $\nu(\nu + 1)/2$ linear independent functionals of the variance and covariance components in $\mathrm{cov}\{\mathbf{d}\}$ can be uniquely determined from the measurements, where ν is the number of redundant measurements.

Hence, using eq. (9), the minimum variance unbiased estimate of least-squares solution for the unknown parameter $\hat{\mathbf{m}}$ is given by

$$\hat{\mathbf{m}} = (\mathbf{G}^{\mathrm{T}}\mathrm{cov}\{\mathbf{d}\}^{-1}\mathbf{G})^{-1}\mathbf{G}^{\mathrm{T}}\mathrm{cov}\{\mathbf{d}\}^{-1}\mathbf{d}, \tag{19}$$

where $\mathrm{cov}\{\mathbf{d}\} \in \mathbb{R}^{N\times N}$ is the estimated covariance matrix of observations. Furthermore, the uncertainty of the unknown parameters can be obtained by

$$\mathrm{cov}\{\hat{\mathbf{m}}\} = (\mathbf{G}^{\mathrm{T}}\mathrm{cov}\{\mathbf{d}\}^{-1}\mathbf{G})^{-1} \text{ subject to } \mathrm{cov}\{\hat{\mathbf{m}}\} \in \mathbb{R}^{\mathcal{X}\times\mathcal{X}} \tag{20}$$

and the misfit (or residual) vector in observation space is given by

$$\hat{\mathbf{e}} = (\mathbf{d} - \mathbf{G}\hat{\mathbf{m}})^{\mathrm{T}}\mathrm{cov}\{\mathbf{d}\}^{-1}(\mathbf{d} - \mathbf{G}\hat{\mathbf{m}}). \tag{21}$$

For the most simple case of the inverse problem with constant-diagonal data covariance matrix and unknown scale factor (or variance factor) σ_0, we have $\mathrm{cov}\{\mathbf{d}\} = \sigma_0^2\mathrm{I}$, where $\mathrm{I} \in \mathbb{R}^{N\times N}$ is the identity matrix. Furthermore,

$$\hat{\mathbf{m}} = (\mathbf{G}^{\mathrm{T}}\mathbf{G})^{-1}\mathbf{G}^{\mathrm{T}}\mathbf{d}, \tag{22}$$

where

$$\mathrm{cov}\{\hat{\mathbf{m}}\} = \hat{\sigma}_0^2(\mathbf{G}^{\mathrm{T}}\mathbf{G})^{-1}, \tag{23}$$

Table 1. Deviatoric moment tensor solutions reported for Zakynthos, Ionian Sea, earthquake 2018. The earthquake was recorded by various agencies (e.g. USGS, NOA, GCMT) and by Sokos *et al.* (2020).

	Nodal Plane 1					Nodal Plane 2		
Agency	Strike (deg)	Dip (deg)	Rake (deg)	DC (per cent)	CLVD (per cent)	Strike (deg)	Dip (deg)	Rake (deg)
USGS	109	82	52	76	−24	9	39	167
NOA	108	85	41	39	−61	14	49	174
GCMT	114	83	63	64	−36	11	28	165
Sokos *et al.* (2020)	113	80	50	43	−57	12	41	165

in which the least-squares estimate of the unknown variance factor of the unit weight is given as

$$\hat{\sigma}_0^2 = \frac{\hat{\mathbf{e}}}{\nu}, \tag{24}$$

where ν is the number of redundant measurements. The redundant measurements depend on number of stations, the number of independent samples per component (frequency range) and rank of design matrix (**G**). Moreover, in detail, the value of variance factor is obtained using redundant measurements ν, namely $\nu = n_f - n_p + r_d$, where n_f is the number of independent observation equations (number of stations × number of components per each station × number of independent samples per component), n_p is the number of inverted parameters and r_d is the rank deficiency of matrix **G**. However, the drawback of the simplified approach in estimating covariance matrix $\mathrm{cov}\{\mathbf{d}\} = \hat{\sigma}_0^2\mathrm{I}$ is that it could not give any information about the cross-covariance elements. A flowchart of the implementation of data covariance matrix estimation is illustrated in Fig. 1.

4 TESTS ON SYNTHETIC DATA

To illustrate the inversion method's performance, we conducted tests with the 2018 M_w 6.8 Zakynthos earthquake (e.g. Cirella *et al.* 2020; Sokos *et al.* 2020; Fig. 2). The Zakynthos earthquake of 2018 was recorded by broad-band and strong-motion networks and provided an opportunity to investigate the activated fault structure. Deviatoric moment tensor solutions were reported for this earthquake by local and global agencies [e.g. the United States Geological Survey (USGS), https://earthquake.usgs.gov; National Observatory of Athens (NOA), http://www.gein.noa.gr; Global Centroid Moment Tensor (GCMT), https://www.globalcmt.org] and investigated in detail by Sokos *et al.* (2020). Moment tensor solutions indicate mixed source mechanism of a strike-slip to thrust type, and they have significant non-DC component (see Table 1). The significant non-DC contribution is represented by a large and negative compensated linear vector dipole component (CLVD) that is attributed, in this case, to a complex faulting (Sokos *et al.* 2020). Indeed, the region is under subhorizontal southwest–northeast compression, enabling mixed thrust faulting and strike-slip faulting.

4.1 Experiments with Gaussian white noise

Synthetic data for the inversion test were computed by the discrete wavenumber method (Bouchon 1981), assuming a Dirac delta function as the source time function and pure shear mechanism with strike/dip/rake (deg) angles 13/40/171. Full seismic moment tensor is parametrized by six elementary moment tensors ($\boldsymbol{M}1 \ldots \boldsymbol{M}6$). Full $\boldsymbol{M}$ is then composed of their linear combination described by six coefficients. The waveforms were filtered by Butterworth bandpass filter with corner frequencies 0.02–0.1 Hz. In analogy to Hingee *et al.* (2011), the uncorrelated pseudo-random white noise traces were added to the synthetic data in amounts between 5 and 20 per cent, scaled by the maximum absolute value of amplitude. More specifically, to create noisy waveforms, time-series were perturbed by Gaussian random values between −1 and 1. In particular, we added white noise of 20 per cent maximum amplitudes associated with individual components of LTHK station, 15 per cent for LCHA and ZARA stations, 5 per cent for components of MTHA, FSK, GUR and PDO stations. In Fig. 3, we show the experiments with white noise, where the synthetic waveform data with 100 per cent DC were inverted into the focal mechanism of 82 per cent DC and strike/dip/rake angles 14/38/174 (deg) with variance factor $4.3 \times 10^{-6}(\mathrm{m}^2)$. The associated Kagan's angle histogram, DC components, and waveforms with noise and synthetic waveforms without noise are also illustrated. Histogram of Kagan's angle calculated with each solution compares to best-fit solution (Kagan 1991).

In order to test the efficiency of the inversion method, we have considered three different types of covariance matrix: diagonal matrix, block-diagonal matrix and full matrix. (I) Diagonal matrix that contains variance (dispersion) of an individual component as

$$\mathrm{cov}\{\mathbf{d}\} = \begin{bmatrix} \mathrm{cov}\{\mathbf{d}_1\} & \mathbf{0} & \cdots & \mathbf{0} \\ \mathbf{0} & \mathrm{cov}\{\mathbf{d}_2\} & \cdots & \mathbf{0} \\ \mathbf{0} & \vdots & \ddots & \vdots \\ \mathbf{0} & \mathbf{0} & \mathbf{0} & \mathrm{cov}\{\mathbf{d}_K\} \end{bmatrix} \quad \text{subject to } \mathrm{cov}\{\mathbf{d}\} \in \mathbb{R}^{N\times N}, \tag{25}$$

where K is the number of stations, $\mathrm{cov}\{\mathbf{d}_i\} = \mathrm{diag}([\sigma_{E_i}^2\mathbf{I}, \sigma_{N_i}^2\mathbf{I}, \sigma_{Z_i}^2\mathbf{I}])$ and $(\sigma_{E_i}^2, \sigma_{N_i}^2, \sigma_{Z_i}^2)$ are the variances of the individual components of ith station. (II) Block-diagonal matrix considering cross-covariance among all three components at each station, which constructed same as eq. (25), whereas

$$\mathrm{cov}\{\mathbf{d}_i\} = \begin{bmatrix} \sigma_{E_i}^2\mathbf{I} & \sigma_{E_iN_i}\mathbf{I} & \sigma_{E_iZ_i}\mathbf{I} \\ \sigma_{N_iE_i}\mathbf{I} & \sigma_{N_i}^2\mathbf{I} & \sigma_{N_iZ_i}\mathbf{I} \\ \sigma_{Z_iE_i}\mathbf{I} & \sigma_{Z_iN_i}\mathbf{I} & \sigma_{Z_i}^2\mathbf{I} \end{bmatrix}. \tag{26}$$

(III) Full covariance matrix:

$$\mathrm{cov}\{\mathbf{d}\} = \begin{bmatrix} \mathrm{cov}\{\mathbf{d}_1\} & \mathrm{cov}\{\mathbf{d}_1,\mathbf{d}_2\} & \cdots & \mathrm{cov}\{\mathbf{d}_1,\mathbf{d}_K\} \\ \mathrm{cov}\{\mathbf{d}_2,\mathbf{d}_1\} & \mathrm{cov}\{\mathbf{d}_2\} & \cdots & \mathrm{cov}\{\mathbf{d}_2,\mathbf{d}_K\} \\ \vdots & \vdots & \ddots & \vdots \\ \mathrm{cov}\{\mathbf{d}_K,\mathbf{d}_1\} & \mathrm{cov}\{\mathbf{d}_K,\mathbf{d}_2\} & \cdots & \mathrm{cov}\{\mathbf{d}_K\} \end{bmatrix}, \tag{27}$$

where $\mathrm{cov}\{\mathbf{d}_i, \mathbf{d}_j\}$ are the (co)variance components between the ith station and the jth station.

Left-hand panels of Fig. 4 show inversion test with diagonal covariance matrix. Histogram of the Kagan's angles illustrated improving resolvability of a DC source after estimating the variance

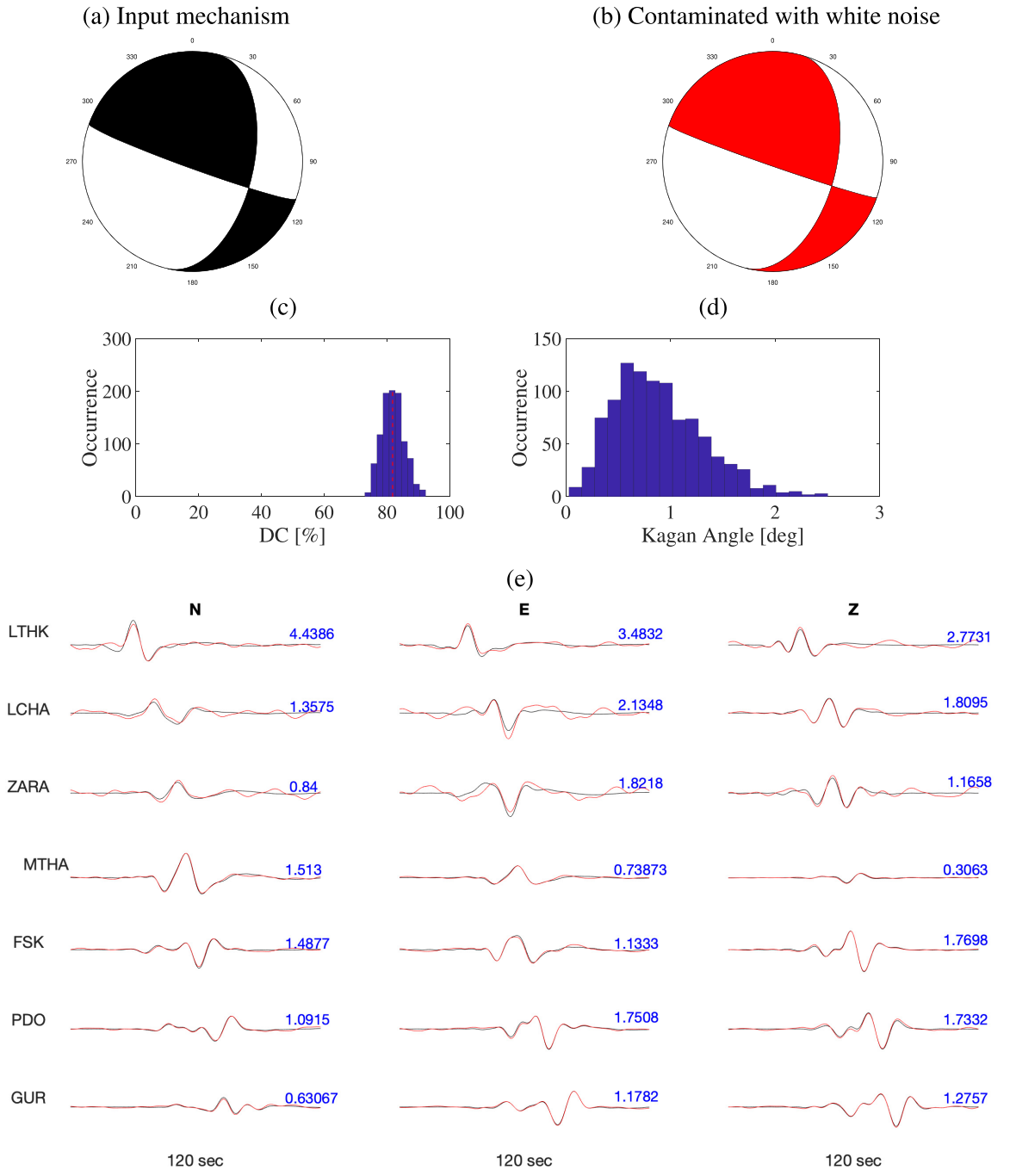

Figure 3. Experiments with Gaussian white noise: (a) original focal mechanism [with strike/dip/rake angles 13/40/171(deg)] used to generate synthetic data with 100 per cent DC, (b) focal mechanism from the MT inversion (without covariance matrix) for synthetic data contaminated with white noise with strike/dip/rake angles 14/38/174(deg) and 82 per cent DC, (c) histogram of DC component, (d) Kagan's angles and (e) waveforms with noise (red) and synthetic waveforms without noise (black). The histograms are built from 1000 random samples of the posterior PDF to visualize the estimated parameter uncertainty. Peak simulated displacements (cm) are shown over the horizontal axis with blue numbers.

matrix. According to Fig. 4(a), the maximum variance could be seen by the LTHK, LCHA and ZARA station's components, which have largest displacement values. The middle panels of Fig. 4 show the estimated focal mechanism of strike/dip/rake angles associated with the block-diagonal data covariance matrix. Again, the strongest features of cross-covariance among all three pairs of components could be seen in LTHK, LCHA and ZARA stations (Fig. 4b). The right-hand panels of Fig. 4 presents the inversion test with the full covariance matrix. It shows the lower absolute values of covariance (with positive and negative signs) between the components of LTHK and LCHA, and ZARA stations (compare Figs 4b and c). This is caused by the presence of interstation cross-covariance (covariance between each pair of stations) and intercomponent cross-covariance (covariance between north, east and vertical components of individual stations), which introduce an additional interstation dependency. Further, according to Hallo & Gallovič (2016),

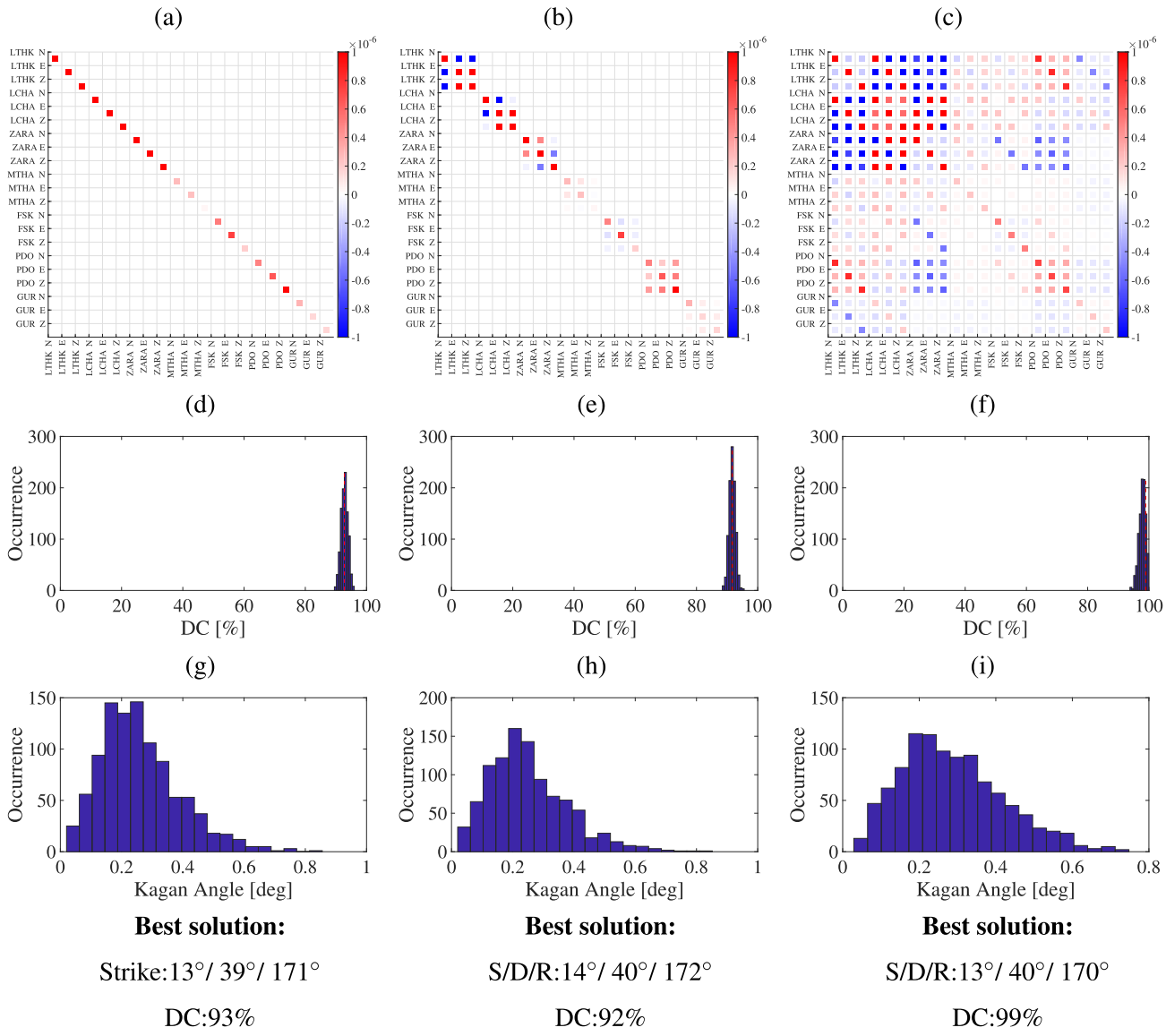

Figure 4. White noise synthetic data tests for diagonal covariance matrix (a), block-diagonal covariance matrix (b), full covariance matrix (c), and the associated DC component (d)–(f), the related Kagan's angles (g)–(i) and maximum likelihood solutions (see the text). The histograms are built from 1000 random samples of the posterior PDF to visualize the estimated parameter uncertainty. The elements of main diagonals associated with different types of matrices, namely diagonal, block-diagonal and full covariance matrices, are different because, in the estimation of each kind of covariance matrices, the cofactor matrices and number of unknowns are different.

negative covariance means that signals are anticorrelated. By comparing the results of this test with the target (input) focal mechanism, it can be concluded that our full covariance matrix has a reliable performance.

4.2 Experiments with coloured (correlated) noise

We simulated waveform for the same focal mechanism as in the previous example and added coloured noise of the same spectral content to all stations with their associated ratios, as described in Section 4.1 (20 per cent of maximum amplitudes associated with individual components of LTHK station, 15 per cent for components of LCHA and ZARA stations, 5 per cent for components of MTHA and FSK, and PDO stations). In this synthetic test, we study whether the covariance matrix of the data is detectable by MLE's method and investigate its effect on the resolvability of the $\boldsymbol{M}$ inversion. The coloured noise characterized by power-law models, where the spectral amplitude is assumed to vary as $F(f) \propto f^{-\kappa}$, where f is the frequency and κ is the power-law index. For instance, the white noise is defined when $\kappa = 0$ and time-dependent noise can be represented by random walk that is called red noise ($\kappa = 2$). In synthetic data test with colored noise, we used $\kappa = 2$ to generate correlated noise.

Correspondingly, Fig. 5 shows inversion test without covariance matrix using synthetic data perturbed by the colored noise. In this test we inverted synthetic waveform data with 100 per cent DC to the focal mechanism of 84 per cent DC and strike/dip/rake angles 8/36/170 (deg) with variance factor 1.45×10^{-5} (m^2). The associated Kagan's angles, DC components histogram, and waveforms with noise and synthetic waveforms without noise are also

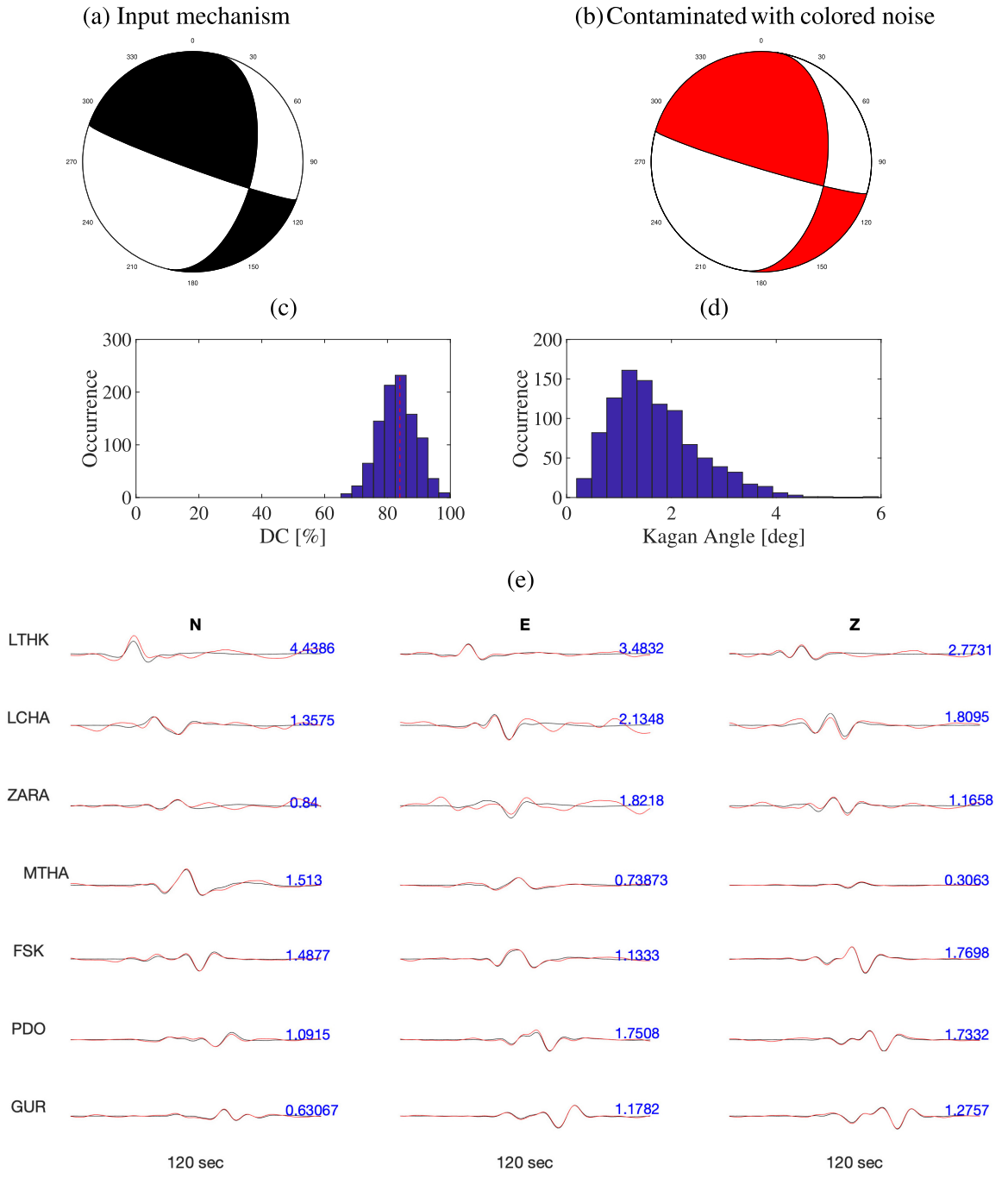

Figure 5. Experiments with coloured noise: (a) original focal mechanism [with strike/dip/rake angles 13/40/171(deg)] used to generate synthetic data with 100 per cent DC, (b) focal mechanism from the MT inversion (without covariance matrix) for synthetic data contaminated with coloured noise with strike/dip/rake angles 8/36/170(deg) with 84 per cent DC, (c) DC component, (d) Kagan's angles, (e) DC mechanism nodal planes and (d) waveforms with noise (red) and synthetic waveforms without noise (black). Peak simulated displacements (cm) are shown over the horizontal axis with blue numbers.

illustrated. Fig. 6 shows inversion tests using three different types of covariance matrices: diagonal covariance matrix, block-diagonal covariance matrix, full covariance matrix, and the resultant focal mechanisms.

The proposed method's performance could be compared using two different metrics: (i) unbiasedness of the MLE estimator, namely $E\{\hat{\mathbf{m}}\} - \mathbf{m}$ and (ii) minimum variance of the estimator MLE, namely the minimum uncertainty of the resultant parameters. The former one could be obtained using the comparing of simulated strike/dip/rake angles [13/40/171 (deg) and 100 per cent DC] with the best of inverted solutions by the diagonal, block-diagonal and full covariance matrices, which are illustrated by Fig. 6. The second one is the uncertainty of parameters which could be described by Kagan's angle. According to Fig. 6, the small values of Kagan's angles histogram show that all acceptable solutions (1000 samples) are less scattered comparing to the solution without covariance matrix in Fig. 5(d). It means that a reliable estimate of the uncertainty of the MT parameters is revealed

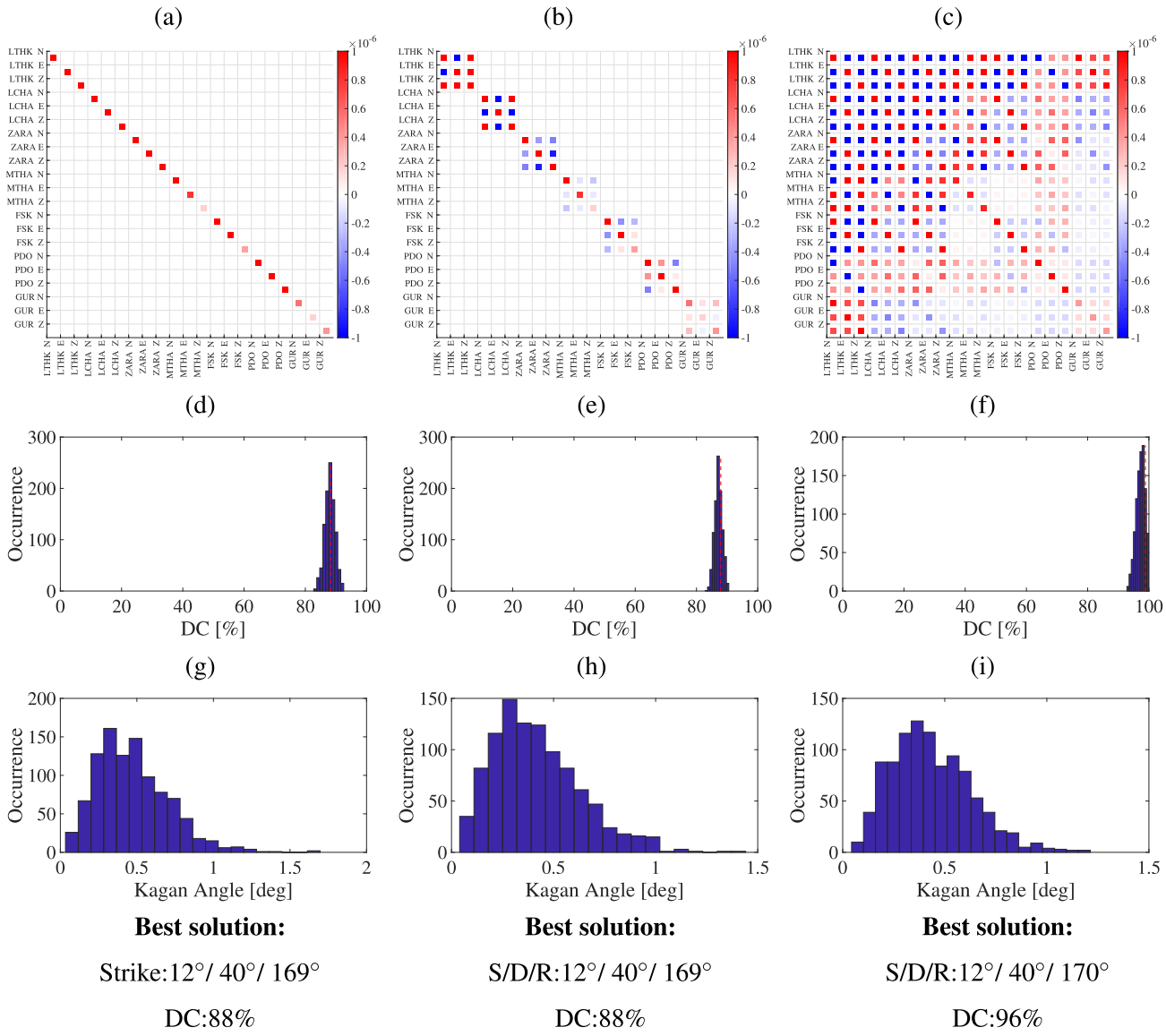

Figure 6. Coloured noise synthetic data tests for diagonal covariance matrix (a), block-diagonal covariance matrix (b), full covariance matrix (c), and the associated DC component (d)–(f), the related Kagan's angles (g)–(i) and maximum likelihood solutions (see the text).

when employing the diagonal, block-diagonal and full covariance matrices.

5 REAL DATA INVERSION

To evaluate the performance of the proposed approach, we applied it to real waveform data of 2018 M_w 6.8 Zakynthos earthquake. The waveforms were filtered by Butterworth bandpass filter between 0.02 and 0.1 Hz and then downsampled to 1.25 Hz sampling rate. We perform MT inversion test using the velocity model proposed by Haslinger *et al.* (1999) for our study area. Fig. 7 shows results of the inversion without covariance matrix with variance factor 2×10^{-5} (m^2) (constant-diagonal matrix) using fixed hypocenter location (latitude/longitude 37.27° /20.43°) with depth 12 km and origin time of 22:54:47.5 UTC (in which we fixed the depth and origin time at values obtained in the location procedure). Our resultant solution has nodal plane of strike/dip/rake (deg) angles 13/40/171 with 33 per cent DC and −61 per cent CLVD with variance reduction (VR) of 0.53 [Variance reduction is defined as $VR = 1 - \Sigma(d-s)^2/\Sigma d^2$, where d and s are the observed and synthetic waveforms (Sokos & Zahradník 2013)]. The solution is in agreement with other agencies, for example, NOA (see Table 1), reporting 39 per cent DC and −60 per cent CLVD. We implemented the proposed covariance matrix estimation for the real waveforms according to the former categorized diagonal covariance matrix, block-diagonal covariance matrix, and full covariance matrix (as shows by Fig. 1). Fig. 8 shows the results of these inversion tests. The estimated focal mechanism of 67 per cent DC and -31 per cent CLVD associated with the estimated diagonal covariance matrix is a strike/dip/rake (deg) angles 12/32/163 with VR value of 0.55. In Fig. 7, the diagonal terms equal 2×10^{-5}(m^2) for all stations and all three components. However, the estimated diagonal terms in Fig. 8(a) are in the range of 1.41×10^{-6} (associated with Z components of MTHA station) up to 1.35×10^{-4} (associated with N components of LTHK station). Hence, that causes the difference in DC and CLVD histograms of the results. The estimated focal

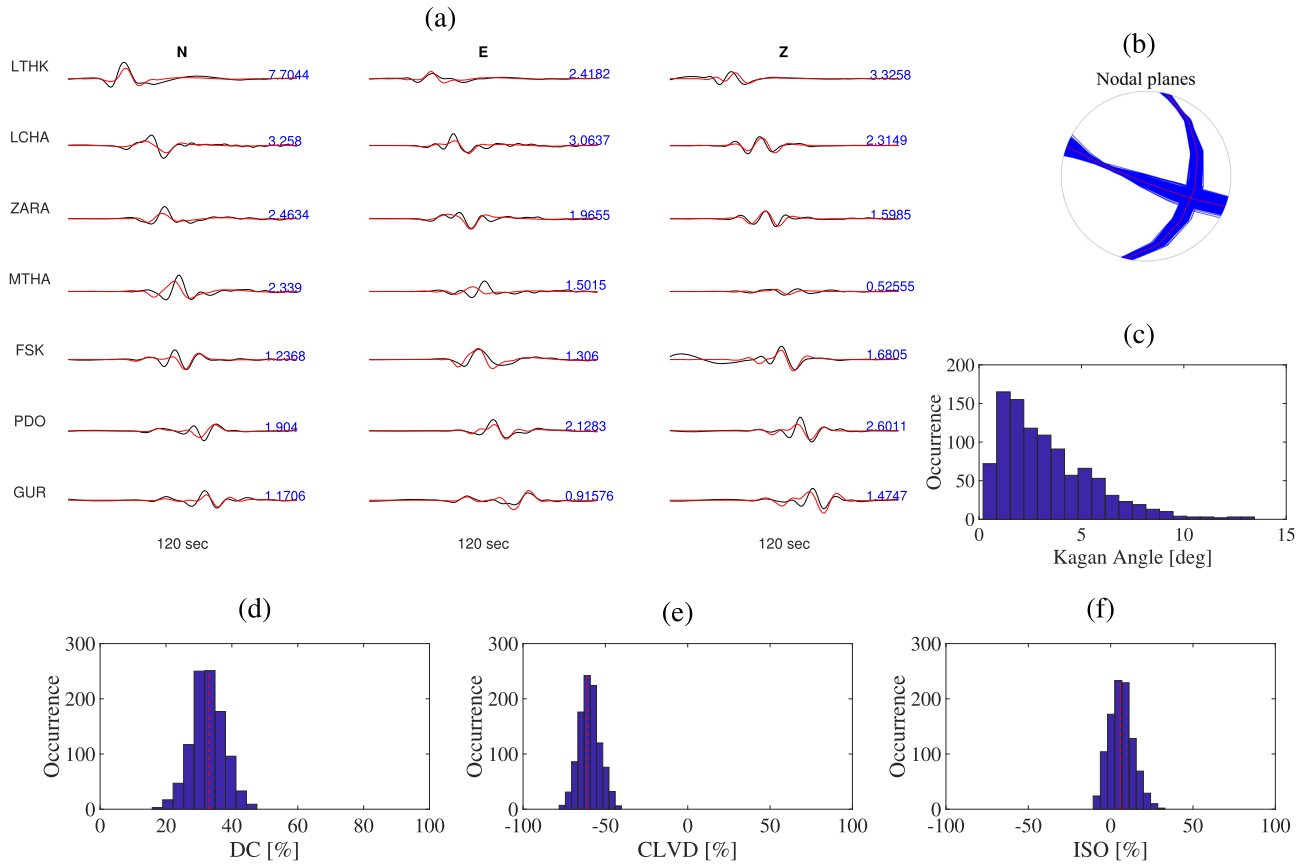

Figure 7. Inversion of the real data using constant-diagonal covariance matrix: (a) simulated waveforms (red) and observed waveforms (black) with variance reduction of 0.53. Peak displacements (cm) are shown over the horizontal axis with blue numbers, (b) DC mechanism nodal planes, (c) Kagan's angles, (d)-(f) histogram of DC, CLVD and ISO components. The maximum likelihood solution (in red) has strike/dip/rake (deg) angles 13/40/171, 33 per cent DC and -61 per cent CLVD with variance factor 2×10^{-5} (m^2). The histograms are built from 1000 random samples of the posterior PDF to visualize the estimated parameter uncertainty.

mechanism of 92 per cent DC and −3 per cent CLVD associated with the estimated block-diagonal covariance matrix is strike/dip/rake (deg) angles 16/32/167 with VR of 0.53. Accordingly, the estimated focal mechanism of 69 per cent DC and −23 per cent CLVD associated with the estimated full covariance matrix is a strike/dip/rake (deg) angles 19/34/177 with VR value of 0.47. Here, the ensemble of the solutions is obtained by random sampling the posterior PDF.

6 CONCLUSION AND DISCUSSION

Using the MLE as a standard method for the minimum-variance unbiased estimation of the data covariance matrix, we estimated three different covariance matrix structures for synthetic and real data sets of the event, 2018 M_w 6.8 Zakynthos (Ionian Sea, Greece) earthquake. The outcomes of the synthetic analysis confirmed those properties of the MLE estimator in the estimation of the unknown parameters (and their uncertainties) in terms of accuracy and precision, respectively. Later, the method is applied for the real data sets of the event with a focal mechanism of strike/dip/rake (deg) angles 13/40/171 of the 33 per cent DC and −61 per cent CLVD. In the case of inversion using the estimated full covariance matrix, we obtained a solution having strike/dip/rake (deg) angles 19/34/177 with 69 per cent DC and −23 per cent CLVD. Accordingly, the results of the real data inversion with the diagonal, block-diagonal and full covariance matrices suggest that the significant negative CLVD component is a reliable feature of the 6.8 Zakynthos earthquake (that is in accord with Sokos et al. 2020). The is due to the estimated full covariance matrix captured the effects of propagated random data errors in the inversion process. It should be noted that our covariance matrices do not include intersample correlations (interrelation of the data temporal samples). This is a difference compared to other published approaches (e.g. Duputel *et al.* 2012; Mustać & Tkalčić 2016; Vackář *et al.* 2017). Hence, we prefer our approach because the drawbacks of their procedures are that, mathematically, they are biased and has no property of minimum variance. In consistent, according to Koch (1986), our estimator is unbiased and has a minimum variance. In each real application, it would be good to perform a specific synthetic test (resembling the real situation) and, based on that case-specific synthetic test, decide which kind of covariance matrix (diagonal, block-diagonal or full) should be used in that particular application.

ACKNOWLEDGEMENTS

The data for the focal mechanism solutions provided by various agencies: NOA (http://www.ge in.noa.gr), USGS (https://earthquake.usgs.gov) and GCMT (https://www.globalcmt.org). Waveform data were sourced from the corresponding Observatories

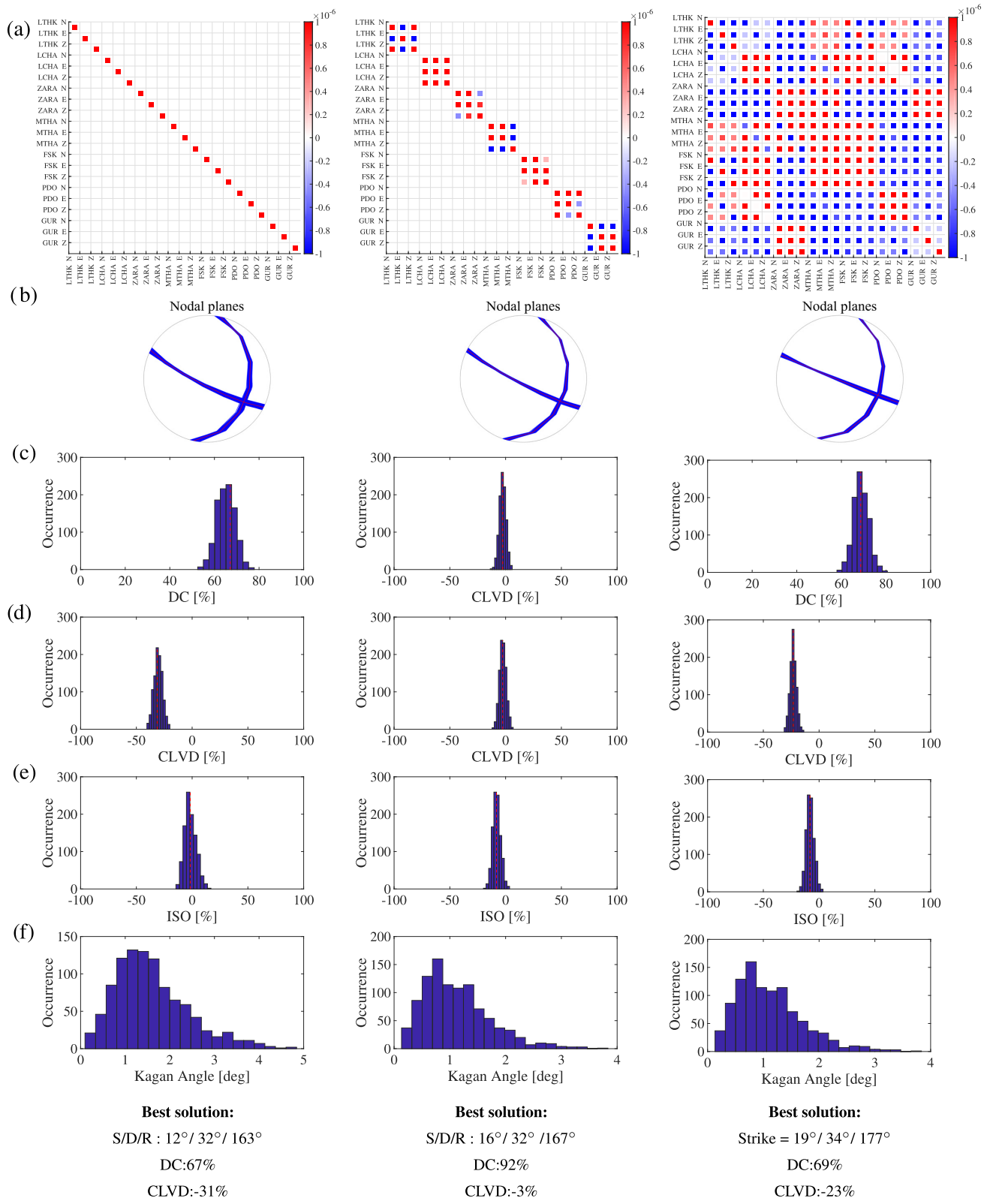

Figure 8. Real data inversion tests for diagonal (left column), block-diagonal (middle column) and full covariance matrix (right column). Ensemble displayed in terms of nodal planes of all the solutions in row (b). Histograms in rows (c), (d) and (e) show DC, CLVD and ISO components and row (f) related Kagan's angle. Last row is the maximum likelihood solutions (see the text) corresponding to the use of different type of the data covariance matrix.

and Research Facilities for European Seismology (ORFEUS) European Integrated Data Archive (EIDA) node (http://www.orfeus-eu.org/eida) operated by the National Observatory of Athens (http://eida.gein. noa.gr).

DATA AVAILABILITY

For easier implementation in other researchers' codes, we release open source codes for computing all the types of the proposed covariance matrices for the 2018 M_w 6.8 Zakynthos (Ionian Sea, Greece) earthquake. The codes can be downloaded from https://github.com/HKheiri/Covariance-matrix.git.

REFERENCES

Aki, K. & Richard, P.G., 2002. *Quantitative Seismology,* University Science Books.

Bouchon, M., 1981. A simple method to calculate Green's functions for elastic layered media, *Bull. seism. Soc. Am.,* **71**(4), 959–971.

Cirella, A. *et al.*, 2020. The 2018 M_w 6.8 Zakynthos (Ionian Sea, Greece) earthquake: seismic source and local tsunami characterization, *Geophys. J. Int.,* **221**(2), 1043–1054.

Duputel, Z., Rivera, L., Fukahata, Y. & Kanamori, H., 2012. Uncertainty estimations for seismic source inversions, *Geophys. J. Int.,* **190**(2), 1243–1256.

Duputel, Z., Agram, P.S., Simons, M., Minson, S.E. & Beck, J.L., 2014. Accounting for prediction uncertainty when inferring subsurface fault slip, *Geophys. J. Int.,* **197**(1), 464–482.

Grafarend, E. & Awange, J., 2012. *Applications of Linear and Nonlinear Models,* Springer-Verlag.

Hallo, M. & Gallovič, F., 2016. Fast and cheap approximation of green function uncertainty for waveform-based earthquake source inversions, *Geophys. J. Int.,* **207**(2), 1012–1029.

Hallo, M., Asano, K. & Gallovič, F., 2017. Bayesian inference and interpretation of centroid moment tensors of the 2016 Kumamoto earthquake sequence, Kyushu, Japan, *Earth Planets Space,* **69**(1), doi:10.1186/s40623-017-0721-4.

Haslinger, F. *et al.*, 1999. 3D crustal structure from local earthquake tomography around the Gulf of Arta (Ionian region, NW Greece), *Tectonophysics,* **304**(3), 201–218.

Hingee, M., Tkalčić, H., Fichtner, A. & Sambridge, M., 2011. Seismic moment tensor inversion using a 3D structural model: applications for the Australian region, *Geophys. J. Int.,* **184**(2), 949–964.

Kagan, Y., 1991. 3-D rotation of double-couple earthquake sources, *Geophys. J. Int.,* **106**(3), 709–716.

Kikuchi, M. & Kanamori, H., 1986. Inversion of complex body waves-II, *Phys. Earth planet. Inter.,* **43**(3), 205–222.

Koch, K.R., 1986. Maximum likelihood estimate of variance components, *Bull. Geod.,* **60**(4), 329–338.

Koch, K.-R., 1999. *Parameter Estimation and Hypothesis Testing in Linear Models,* Springer.

Minson, S.E., Simons, M. & Beck, J.L., 2013. Bayesian inversion for finite fault earthquake source models I—theory and algorithm, *Geophys. J. Int.,* **194**(3), 1701–1726.

Monelli, D., Mai, P.M., Jónsson, S. & Giardini, D., 2009. Bayesian imaging of the 2000 western Tottori (Japan) earthquake through fitting of strong motion and GPS data, *Geophys. J. Int.,* **176**(1), 135–150.

Mustać, M. & Tkalčić, H., 2016. Point source moment tensor inversion through a Bayesian hierarchical model, *Geophys. J. Int.,* **204,** 311–323.

Sokos, E. & Zahradník, J., 2013. Evaluating centroid-moment-tensor uncertainty in the new version of ISOLA software, *Seismol. Res. Lett.,* **84**(4), 656–665.

Sokos, E., Gallovič, F., Evangelidis, C.P., Serpetsidaki, A., Plicka, V., Kostelecký, J. & Zahradník, J., 2020. The 2018 M_w 6.8 Zakynthos, Greece, earthquake: dominant strike-slip faulting near subducting slab, *Seismol. Res. Lett.,* **91**(2A), 721–732.

Spudich, P., Cirella, A., Scognamiglio, L. & Tinti, E., 2019. Variability in synthetic earthquake ground motions caused by source variability and errors in wave propagation models, *Geophys. J. Int.,* **219**(1), 346–372.

Tarantola, A. & Valette, B., 1982. Inverse problems = quest for information, *J. Geophys.,* **50**(1), 159–170.

Vackář, J., Burjánek, J., Gallovič, F., Zahradník, J. & Clinton, J., 2017. Bayesian ISOLA: new tool for automated centroid moment tensor inversion, *Geophys. J. Int.,* **210**(2), 693–705.

Valentine, A.P. & Trampert, J., 2012. Assessing the uncertainties on seismic source parameters: towards realistic error estimates for centroid-moment-tensor determinations, *Phys. Earth planet. Inter.,* **210–211,** 36–49.

Vasco, D.W., 1990. Moment-tensor invariants: searching for non-double-couple earthquakes, *Bull. seism. Soc. Am.,* **80**(2), 354–371.

Šílený, J., Panza, G.F. & Campus, P., 1992. Waveform inversion for point source moment tensor retrieval with variable hypocentral depth and structural model, *Geophys. J. Int.,* **109**(2), 259–274.

Wéber, Z., 2006. Probabilistic local waveform inversion for moment tensor and hypocentral location, *Geophys. J. Int.,* **165**(2), 607–621.

Xu, P., Liu, Y., Shen & Fukuda, Y., 2007. Estimability analysis of variance and covariance components, *J. Geod.,* **81,** 593–602.

Yagi, Y. & Fukahata, Y., 2008. Importance of covariance components in inversion analyses of densely sampled observed data: an application to waveform data inversion for seismic source processes, *Geophys. J. Int.,* **175**(1), 215–221.

Yagi, Y. & Fukahata, Y., 2011. Introduction of uncertainty of green's function into waveform inversion for seismic source processes, *Geophys. J. Int.,* **186**(2), 711–720.

Zahradník, J. & Custódio, S., 2012. Moment tensor resolvability: application to southwest Iberia, *Bull. seism. Soc. Am.,* **102**(3), 1235–1254.